Supporting Online Material for

Proton Radiography of Inertial Fusion Implosions

J. R. Rygg, F. H. Séguin, C. K. Li, J. A. Frenje, M. J.-E. Manuel, R. D. Petrasso,*
R. Betti, J. A. Delettrez, O. V. Gotchev, J. P. Knauer, D. D. Meyerhofer, F. J. Marshall,
C. Stoeckl, W. Theobald

*To whom correspondence should be addressed. E-mail: petrasso@psfc.mit.edu

Published 29 February 2008, *Science* **319**, 1223 (2008)

DOI: 10.1126/science.1152640

This PDF file includes:

Supplementary Material:
Proton Radiography of Inertial Fusion Implosions

J. R. Rygg[1,*], F. H. Séguin[1], C. K. Li[1], J. A. Frenje[1], M. J.-E. Manuel[1], R. D. Petrasso[1,†], R. Betti[2], J. A. Delettrez[2], O. V. Gotchev[2], J. P. Knauer[2], D. D. Meyerhofer[2], F. J. Marshall[2], C. Stoeckl[2], W. Theobald[2]

[1]Plasma Science and Fusion Center, Massachusetts Institute of Technology, Cambridge, MA 02139, USA.
[2]Laboratory for Laser Energetics, University of Rochester, Rochester, NY 14623, USA.
[*]Current address: Lawrence Livermore National Laboratory, Livermore, CA, 94551, USA.
[†]To whom correspondence should be addressed; Email: petrasso@psfc.mit.edu

MATERIALS AND METHODS

All experiments were performed at the OMEGA laser facility (*S1*), which delivers up to 30 kJ in 60 beams at a wavelength of 351 nm. Full beam smoothing (*S2*) was used on each beam to reduce high-mode nonuniformities caused by laser speckle.

A schematic illustration of the proton radiography setup is shown in Fig. 1 in the primary text. The source of monoenergetic protons is a 220-μm radius, 2.2 μm thick spherical glass (SiO_2) shell filled with deuterium (D_2) and helium-3 (^3He) gas (*S3*). This backlighter capsule is illuminated with 17 laser beams, delivering 6.9 kJ energy in a 1-ns pulse, which compresses and heats the gas such that the D-^{3}He fusion reaction, $D + {}^3He \rightarrow {}^4He + p$, proceeds. The protons are quasi-isotropically emitted in a 130 ps pulse (*S4*), at an energy of 15.0 MeV (*S5*), with a spectral width (*S6*) $\Delta E/E < 3\%$, and from a region 45 μm across (*S3*) (see fig. S1). Typical proton yields are 1-4×10^8, and the yields for the OMEGA shots shown in the primary text were 2.9×10^8 (shot 46531) and 3.7×10^8 (shot 46529). The backlighter implosion has not yet been fully optimized for proton yield, pulse duration, or source size.

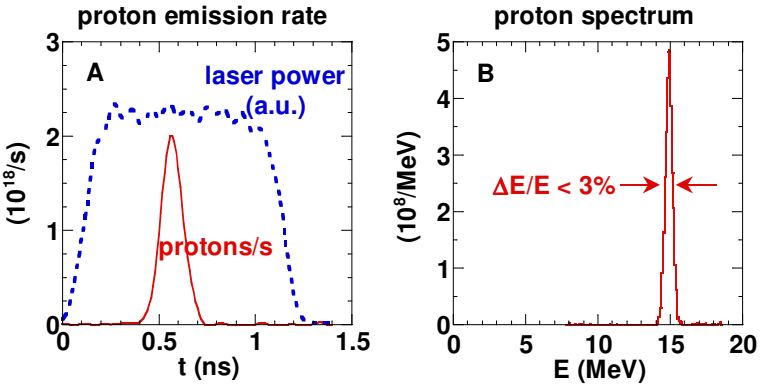

Fig. S1: Measured characteristics of proton emission from the source implosion. Emission history (A) and spectrum (B) of emitted D^{3}He protons from the backlighter capsule on OMEGA shot 46531. The total D^{3}He proton yield was 2.9×10^8. Also shown is the power history of the laser drive (dotted blue line).

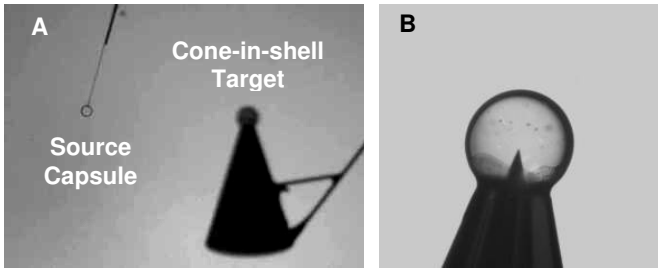

Fig. S2: (A) Pre-implosion snapshot of source and target capsules. (B) A close-up photograph of the cone-in-shell target sphere. See also Fig. 1.

The target imaged is a 430 μm radius, 23-μm-thick spherical plastic (CH) shell with an embedded gold (Au) cone of height 5 mm, thickness 30 μm, and opening angle 35°. The cone ends in a shelf (see fig. S2) where the cone intersects the shell, and a smaller cone tip reaches inward to a distance 40 μm from the capsule center. 40 beams in a spherically symmetric configuration are pointed at the spherical shell; the shell is then directly driven with 14.1-kJ in 1-ns using 36 of those beams (the four beams aimed nearest the cone axis are left off to avoid the laser hitting inside of the cone), for an on-target illumination intensity of 6.7×10^{14} W/cm^2. Because the OMEGA system is optimized for 60-beam spherical drive, the illumination uniformity is degraded in this configuration from <2% to ~7% rms.

The imaging detector is CR-39, a plastic nuclear track detector with sub-micron spatial resolution, low sensitivity to electromagnetic and x-ray noise sources, and energy resolving characteristics (*S6*). The position and energy of every incident proton is recorded. The center of the sphere in the target capsule is placed 1.0 cm from the center of the source capsule, and the detector is located 25 cm from the source, so structure in the target is magnified by a factor $M = 25$ at the detector. The relative timing of source and target-capsule drive beams is adjusted so the backlighter protons arrive at the target capsule at a desired time interval following the onset of target-capsule drive (Fig. 2).

The spatial resolution of the system, neglecting scattering in the target, is limited primarily by the finite source size, and results in convolution of structure in the target plane by a Gaussian of FWHM about 43 μm. Structures smaller than this cannot be observed in the capsule corona without further optimization of the backlighter source.

The energy resolution of the system is about 0.05 MeV, corresponding to an areal density resolution of about 1.5 mg/cm^2. A more thorough analysis of the absolute accuracy of proton energy measurements on the radiographic CR-39, as well as assessment of the effects of angular scattering of protons through plasma in the target plane, is currently in progress.

OTHER RELEVANT WORK

Of direct relevance to this paper, and in support of the presence of the observed field structures, Shiraga *et al.* (S7) and Séguin *et al.* (*S8*) inferred the presence of residual electromagnetic fields outside imploded capsules (exploding pushers and ablatively

driven implosions similar to those studied here, respectively) on the basis of fluence variations in self-emitted, charged fusion products. Furthermore, characterization of capsule assembly and symmetry in ICF-relevant implosions has included extensive use of self-emitted fusion protons (*S9,S6*), including those from implosions of fast-ignition (FI) targets (*S10*). Recently, Li *et al.* (*S3*) suggested that a complementary way of studying implosions and, in particular, the spatial structure of fields and of areal density, is through monoenergetic proton radiography.

Filamentary and jet-like structures were previously observed outside the critical surface using shadowgraphic, interferometric, and faraday rotation techniques by several groups, during laser illumination of both planar targets (*S11*,*S12*), and spherical targets (*S13*,*S14*). As mentioned in the main text, there are substantial differences between the filamentary structures observed by these workers and those reported in this Report: (i) The lateral spatial wavelength of structures was 10 μm, and examination of their data shows no evidence of the ~150 μm spatial scale that we see. (ii) The radial extent of the earlier structures is much smaller and confined, whereas the structures reported here fills the entire field of view. (iii) Fine structures originate in the underdense plasma, while the structures here originate inside the critical surface, even approaching the ablation surface (see fig. S3). (iv) Furthermore, for uniformly illuminated implosions, fields greater than 10 T were not detected (*S15*). In addition, it's useful to point out that one of the unique advantages of the particle probe that we have used is that it is not "cut off" by critical density plasma effects as is the case for optical probes.

Previous studies of laser-capsule interactions using broad-band proton radiography (*S16*) include Borghesi *et al.* (*S17*) and Mackinnon *et al.* (*S18*). Borghesi illuminated a sphere from one side using a single, short (1 ps), intense pulse, and observed filamentary structures similar to those described in the previous paragraph. However, Mackinnon saw no filamentary or focusing fields surrounding a capsule driven with six 1-ns laser beams. The fact that Mackinnon did not see these structures is not presently understood. There are, however, substantial differences in the implosion conditions compared to the current work. For example, MacKinnon used six beams at 1-μm wavelength and 1.5×10^{13} W/cm^2 intensity; herein we used 36 beams at 1/3-μm and 6.7×10^{14} W/cm^2. In addition, Mackinnon's radiographic images were obtained substantially after (~1.5 ns) the end of the driving laser pulse, whereas in the current work, radiographs were obtained shortly after (~0.3 ns) the end of the pulse. If the observed field structures are produced and sustained by the laser (see "possible mechanisms", below), the structures may no longer be detectable 1 ns after their generating source has turned off.

The monoenergetic D^3He fusion proton emission from backlighter capsules has, for the purposes of these experiments, substantial advantages over broad-band, non-isotropic proton emissions associated with intense-laser-beam experiments (*S16*). A single energy provides unambiguous quantitative relationships between proton energy loss through the target and areal density and also between proton trajectory bending and field strengths at the target. Quasi-isotropy allows for imaging of large objects, or even simultaneous imaging of multiple objects in totally different directions [as has been done in other contexts (*S19*)].

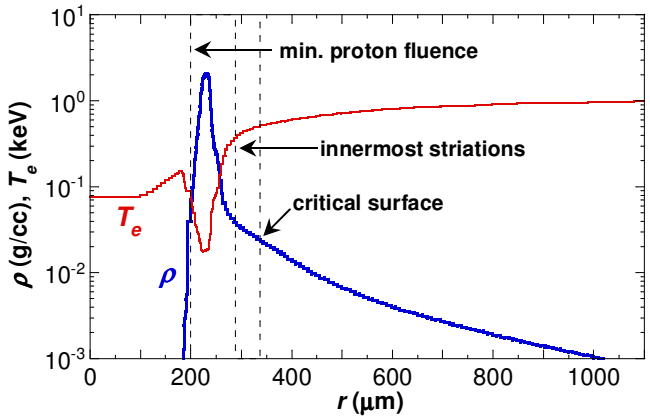

Fig. S3: LILAC (*S20*) simulation of mass density (ρ) and electron temperature (T_e) profiles of the imploding capsule at 1.56 ns, ~0.3 ns after the laser has turned off. At this time, the capsule shell (the region of highest density near 230 μm) is imploding inward at approximately constant speed. The radius corresponding to the observed minimum proton fluence (fig. S4) occurs at the inner shell surface (~200 μm) in the simulation. The innermost striations are observed at about 300 μm (Fig. 3B), well inside the critical density surface (for λ=0.351 μm).

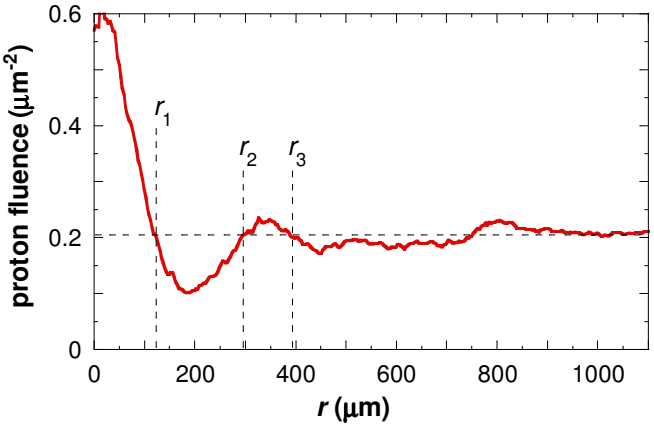

Fig. S4: Reproduction of Fig. 4B, marking the boundaries of the proton fluence enhancement at the center ($r< r_1$), the fluence depression through the capsule limb and *E*-field region ($r_1< r <r_2$), and a secondary fluence enhancement outside the shell ($r_2< r <r_3$). Fluence peaks and troughs in the "far field" region ($r > 430$ μm = initial capsule radius) are the result of filamentary structures. Also marked is the proton fluence of 0.20 protons/μm^2, equal to the far field average fluence. In the absence of a focusing electric field, one would expect that scattering of protons through the capsule limb should deflect an approximately equal number of protons inwards as outwards. The number of protons deflected out of the trough region $r_1< r <r_2$ is about 12,300, calculated as the difference in the number of protons over an azimuthal integral in that region compared to the expected number based on the far field fluence and the area of the region. The number of protons deflected into the inner and outer proton fluence peaks are 8,300 and 4,100, respectively. Therefore, angular scattering through the limb plasma can only account for about half of the protons in the central peak; we invoke the presence of a focusing *E*-field to explain the remainder of the fluence enhancement at the center.

POSSIBLE MECHANISMS

Numerous instabilities that generate magnetic fields in laser-plasma experiments have been identified or proposed (*S21*), and take place over a wide range of plasma conditions. The instabilities generated outside the critical density surface are the collisionless Weibel, thermomagnetic and filamentation instabilities. Just inside the critical surface, the collisional Weibel, $\nabla T \times \nabla n$, and thermomagnetic instabilities will grow. Nernst convection can carry B fields generated by these instabilities inwards (or outwards) (*S21*). The electrothermal instability occurs at higher densities when the mean free path is shorter than the electron skin depth (*S22*). The Rayleigh-Taylor (RT) instability generates B fields at the ablation front (*S23*,*S24*).

Monoenergetic proton radiography of planar foils seeded with RT ripples are currently in progress to investigate the generation and growth of fields by RT processes. Preliminary results have observed of order ~100 Tesla magnitude magnetic fields structures, which appear to be absent when the rippled RT seed is absent from the foil.

An estimate of the RT-induced B-field magnitude can be obtained using the work of Nishiguchi (*S24*). The capsule shell acceleration g can be approximated from the experimental observations as the distance the shell has traveled over one half the square of the time it took to get there, $g = 2(430–215\ \mu m)/(1.5\ ns)^2 \approx 200\ \mu m/ns^2$. The observed transverse spacing between filaments near the capsule surface is typically 150 μm. LILAC simulations (*S20*) show that $L = 10$ μm is typical of the plasma density scale length. From these values, $\sqrt{gk} = 3\times10^9\ s^{-1}$, and $kL = 0.42$. Consulting Figure 1 of Nishiguchi, this gives a peak B-field magnitude of about 300 T at the end of the linear phase of RT growth – only 5 times the observed B field magnitude "averaged" over the width of a filament.

Although RT processes could plausibly generate the observed B fields, other mechanisms can not all be precluded. New experiments using monoenergetic proton radiography will be performed to investigate which instability mechanism(s) are at work. A time sequence of radiographs would enable observation of the onset, growth, and decay of such filamentary structures. Variation of the intensity and other laser conditions could be used to elucidate the origin and any thresholds. Comparison of these radiography results with those from laser-driven solid-plastic capsules, which undergo no acceleration to drive RT growth, would be able to determine if RT is a dominant mechanism.

Whatever the mechanism, magnetic fields generated close to the ablation front would get "frozen in" to the ablating material, and would follow the plasma flow off the capsule surface. If so, structures at the edge of the field of view were actually generated some several hundred picoseconds earlier. Therefore, a history of the filamentary structure as a function of time is available in a single radiographic snapshot.

In regard to the coherent focusing field, the primary text emphasized the possible and likely connection between the central coherent electric field and the pressure gradient at the fuel-shell interface. Yet, another intriguing consequence is that this field could also opportunely reflect hot electrons that otherwise might preheat the fuel. To make such an assessment quantitative would require that we have information about both the evolution

of this coherent field and how it's affected by the laser pulse shape and the capsule itself. (Because of shot limitations, for example, we have so far only investigated the coherent field for the 1-ns square pulse shape, as depicted in Fig 2.) We would also need rather detailed information about the bath of hot electrons, how it is generated, how it depends on pulse shape and the capsule, and, in general, how the hot electron distribution evolves. In the course of exploring the full consequences of the central coherent field, we will investigate this preheat amelioration possibility.

SUPPORTING REFERENCES AND NOTES

S1. T. R. Boehly *et al.*, *Opt. Commun.* **133**, 495-506 (1997).
S2. S. Skupsky, R. S. Craxton , *Phys. Plasmas* **6**, 2157-2163 (1999).
S3. C. K. Li *et al.*, *Rev. Sci. Instrum.* **77**, 10E725 (2006).
S4. J. A. Frenje *et al.*, *Phys. Plasmas* **11**, 2798-2805 (2004).
S5. Hot electrons escaping from the backlighter capsule during laser irradiation results in a capsule charge of several hundred kV, which accelerates the escaping D^3He protons above their 14.7 MeV birth energy. This shift is measured to 0.1 MeV accuracy by the proton spectrometers (*S6*).
S6. F. H. Séguin *et al.*, *Rev. Sci. Instrum.* **74**, 975-995 (2003).
S7. H. Shiraga, T. Mochizuki, C. Yamanaka, *Appl. Phys. Lett.* **37**, 602-604 (1980).
S8. F. H. Séguin *et al.*, *Phys. Plasmas* **9**, 3558-3566 (2002).
S9. H. Azechi *et al.*, *Laser and Particle Beams* **9**, 193-207 (1991).
S10. C. Stoeckl *et al.*, *Plasma Phys. Controlled Fusion* **47**, B859-B867 (2005).
S11. B. Grek *et. al.*, *Phys. Rev. Lett.* **41**, 1811-1814 (1978).
S12. G. Thiell, B. Meyer, *Laser and Particle Beams* **3**, 51-58 (1985).
S13. T. Mochizuki *et. al.*, *Jap. J. Appl. Phys.* **19**, L645-L648 (1980).
S14. O. Willi, P. T. Rumsby, *Opt. Commun.* **37**, 45-48 (1981).
S15. O. Willi, P. T. Rumsby, *Opt. Commun.* **37**, 40-44 (1981).
S16. A. J. Mackinnon *et al.*, *Rev. Sci. Instrum.* **75**, 3531-3536 (2004).
S17. M. Borghesi *et al.*, *Phys. Plasmas* **9**, 2214-2220 (2002).
S18. A. J. Mackinnon *et al.*, *Phys. Rev. Lett.* **97**, 045001 (2006).
S19. C. K. Li *et al.*, *Phys. Rev. Lett.* **99**, 055001 (2007).
S20. J. A. Delettrez *et al.*, *Phys. Rev. A* **36**, 3926-3934 (1987).
S21. M. G. Haines, *Can. J. Phys.* **64**, 912-919 (1986).
S22. M. G. Haines, *Phys. Rev. Lett.* **47**, 917-920 (1981).
S23. K. Mima, T. Tajima, J. N. Leboeuf, *Phys. Rev. Lett.* **41**, 1715-1719 (1978).
S24. A. Nishiguchi, *Jpn. J. Appl. Phys.* **41**, 326-329 (2002).